

FEATURES OF SHOCK WAVE UNSTEADINESS IN SHOCK WAVE BOUNDARY LAYER INTERACTION

L. Agostini

Department of Aeronautics
Imperial College London
London SW7 2AZ, U.K.
l.agostini@imperial.ac.uk

L. Larchevêque

IUSTI
Aix-Marseille University, UMR CNRS 7343
13453 Marseille Cedex 13, France
email

P. Dupont

IUSTI
Aix-Marseille University, UMR CNRS 7343
13453 Marseille Cedex 13, France
email

Introduction

The interactions between a shock wave and a boundary layer arise in several aeronautical applications and have been studied for decades. When separation occurs, they have been shown to be strongly unsteady and the separation shock is moving at very low frequencies. These unsteadiness have a direct influence on the performances of the system and can create strong stress on the structure. Some authors, see for instance Ganapathisubramani *et al.* (2007), have proposed to relate the low frequency shock motions to the upstream perturbations in the incoming boundary layer. On the opposite, others authors including Robinet (2007); Dupont *et al.* (2008); Wu & Martin (2008); Priebe & Martin (2012), have suggested that these perturbations are developing in the downstream part of the interaction. Finally, a recent analysis by Toubert & Sandham (2011) proposed to assimilate the interaction as a low pass filter, with a very low frequency cut off frequency, as initially suggested in the experiments by Plotkin (1975).

The aim of this paper is not to explain the physical mechanism leading to the low frequency shock motions, but to identify their localisations and how the separation shock is influenced. It will be shown that phenomena occurring within the recirculation bubble govern the whole interaction, whatever the frequency range: the shock motions appear to be the mirror of these phenomena developing in the separated zone. An equivalent inviscid scheme of the unsteady interaction is established to describe the whole unsteadiness of the shock system, as well as the downstream unsteady pressure field.

Numerical simulations

A shock reflection on a Mach 2.3 turbulent boundary layer has been considered. The parameters used to perform simulations have been chosen in order to reproduce accurately two interaction configurations installed in the IUSTI's wind tunnel. Large Eddy Simulations are performed using ONERA's FLU3M solver relying on the selective mixed-scale subgrid model, and they are achieved at the

same Reynolds number than the experiments: $Re_{\delta_2} = 5000$, where δ_2 is the momentum thickness of the upstream boundary layer. The computation details and comparisons with experiments have been documented in Agostini *et al.* (2012). We consider here a $9^\circ 5'$ flow deviation, which corresponds to a fully separated flow.

Pressure fluctuations and influence zone

Most of the time resolved measurements available in the literature are restricted to unsteady wall pressure data. In this section, we first present numerical results obtained at the wall, then we will extend these results to whole field.

In figure 1, the dashed line shows the dimensionless main pressure value defined by: $P^* = (P - P_0)/P_0$, where P_0 is the upstream static pressure. The rms streamwise distribution of the low-passed filtered pressure fluctuations ($p_{LF}^* = p_{LF}'/P_0$) is denoted by the full grey line. The cut off frequency f_{LP} of the low pass filter corresponds to a Strouhal number of $S_L = f_{LP}L/U_1 = 0.08$ with L denoting the interaction length and U_1 being the velocity downstream the incident shock. The cut-off frequency allows the extraction of the low frequency unsteadiness of the interaction which have been found to involve frequencies centered around $S_L \simeq 0.03$, see Dupont *et al.* (2006). The longitudinal dimensionless coordinate X^* is defined by $X^* = (X - X_0)/L$, where X_0 is the location of the maximum of the pressure rms to the wall. The rms peak arises where the mean-pressure increase linked to the head shock is stronger. In the case where the turbulent pressure fluctuations are very weak on the either side of the shock wave, the rms values compare with the pressure step across the shock (Δp_s). The shock displacement involves an abrupt increase of the fluctuation values and is consequently scaled on Δp_s in such a way that their rms values are the half of the pressure jump. As these fluctuations are not being produced by turbulent phenomena, they will be referred to as "intermittent". In figure 1, the region labelled *A* is associated with the shock-wave excursion extent. In order to highlight the "intermittent" nature of the pressure fluctuations in zone *A*, at

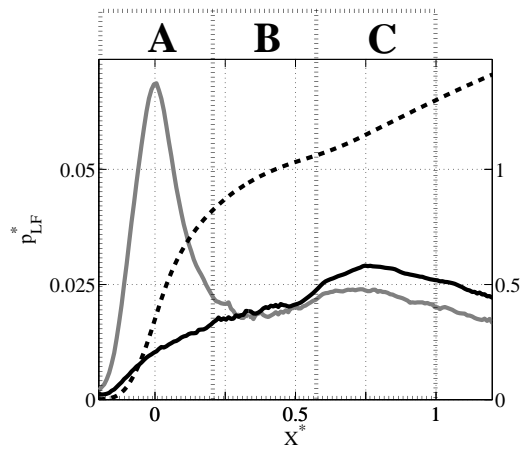


Fig. 1. Streamwise distribution low-frequency wall-pressure rms; grey line: wind tunnel coordinate system; black line: moving frame associated with the head-shock displacement; dashed line: mean pressure (wind tunnel system)

each time step the streamwise pressure profiles were translated in order to be kept steady in the reference frame of the head-shock. The shock displacements have been derived from the time resolved data, and were estimated from locations of maxima of the pressure gradient along the direction normal to the reflected shock. The streamwise profile of the rms values in this frame is denoted by the full black line in figure 1. As expected, the large peak of the rms pressure in the shock motion region (zone A) is strongly reduced by a factor of five. It confirms that the pressure fluctuations are linked to the shock displacements, and related to the large pressure gradient across the head shock. The remaining level (about $p_{LF}^* \approx 0.01$) can be considered as a residual noise, due to the estimation of the shock location. Downstream, the rms values estimated in the shock frame are very close to the value measured in the wind-tunnel frame.

The map of the coherence at $S_L = 0.03$ between the wall pressure fluctuations and the shock position at several altitudes is plotted in figure 2. The coherence functions between wall pressure fluctuations and shock displacements highlights the links independently of any phase between signals. Its value range from 0 to 1, respectively associated to un- and fully correlated signals. The shock altitudes normalized by the shocks-crossing-point altitude H_I are reported on the y-axis. Following results can be derived:

- whatever the shock altitude taken as reference, the coherence level is high between shock motions and pressure variations occurring at the foot of the shock (zone A).
- the coherence is also high between shock displacement and pressure fluctuations occurring in the second part of the separated zone. Moreover, the coherence level increases with shock altitude. This region is labelled C.
- there is a region splitting the separated region in two parts, where the coherence is low, it is labelled B. The region B is also reported on figure 1: it corresponds to the extent where the rms value is minimum in the wind-tunnel system, and where the mean pressure increases more slowly.

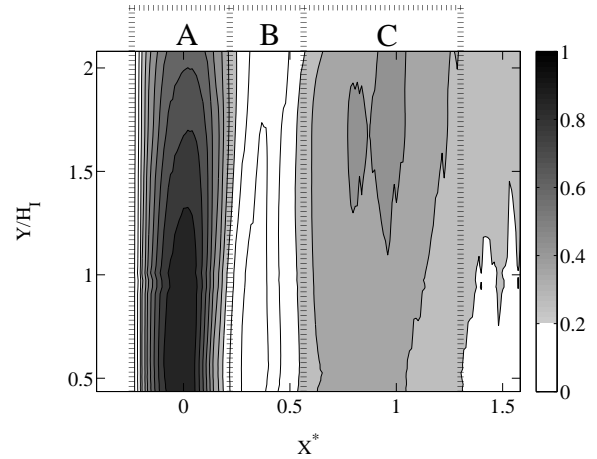


Fig. 2. Map of coherence between the wall pressure fluctuations and the shock position in several altitudes for $S_L = 0.03$.

From numerical simulations, the previous pressure analysis can be extended from the wall to the whole field, thereby defining the zones of influence and their links between each others. The space-time properties of the pressure field are analyzed. The RMS low-pass filtered pressure fluctuations are presented in figure 3(a). The magnitude levels are truncated above 10% of maximum value reached by the intermittent fluctuations. As expected, the maxima rms occur in the head-shock location. More surprisingly, the lowest low frequency pressure variations occur just behind the shock and are lower than 50 Pa, a value being three to four times smaller than the levels observed in the other parts of the interaction. This region splits the interaction into two parts. Downstream of this low level pressure fluctuations region, from $X^* \simeq 0.50$ to 1.20, the rms values are increasing up to 130 Pa in the near wall region as well as in the external flow. Upstream of the interaction, no significant pressure fluctuations at low frequencies are seen in figure 3(a):

it was expected since the Synthetic Eddy Method used to generate inflow conditions in the present simulations, with a distance between the inflow plane and the interaction region of 10δ , which is three times smaller than the useful distance for “super-streaks” to arise, as reported in the literature, see Ganapathisubramani *et al.* (2006)

It arises that, when low frequencies are considered, the interaction can be split in several parts. In order to understand more accurately the spatial organization, the low frequency coherence ($S_L \approx 0.03$) between the shock motions and the pressure fluctuations in the whole field has been carry out, and is plotted in figure 3(b). The signal of the shock position has been defined at $y/H_I \approx 1.2$: it is shown by the white star in the figure. High coherence levels are obtained along the shock wave and in the downstream part of the interaction. Between these two regions, a coherence gap splits the interaction and extends beyond the wall region. Similar results have been obtained from the low-pass-filtered cross correlation in Agostini *et al.* (2012) and show that the shock displacements at low frequency and pressure variations in the second part of the interaction are strongly correlated.

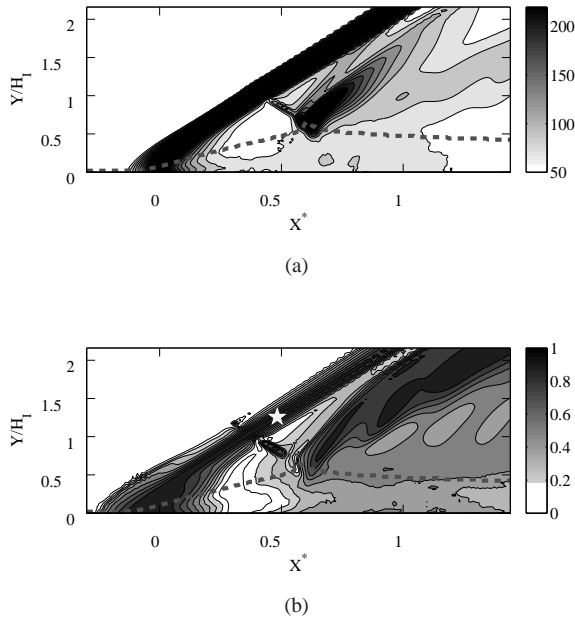


Fig. 3. Features of low frequency pressure fluctuations for the fully separated case: (a) standard deviation of pressure fluctuation occurring at low frequencies $S_L \leq 0.08$, (b) Coherence fields between the shock location and pressure fluctuations low-pass filtered $S_L \approx 0.03$.

Conditional analysis based on the interaction length

In order to analyse only the fluctuations linked to the turbulent phenomena, a conditional analysis based on the shock position was carried out. It aims at eliminating the intermittent pressure fluctuations associated to the shock displacements. In the second part of the bubble, pressure variations occurs and are clearly associated with the shock motions. From the probability density function of the shock positions, only events corresponding to the extrema positions of the shock are considered. Two classes are defined associated respectively with the more upstream positions (15% of the whole samples) and the more downstream ones (15% as well). Piponniau *et al.* (2009) have shown that the exploration lengths of the head shock are strongly linked with the size of the separation bubble: consequently these two classes correspond respectively to the largest and the smallest interaction lengths as well as to the large and small bubbles. To evaluate the pressure fluctuations in the head shock frame, the wall pressure is sampled at a location translated by the shock location associated with the two classes. The conditional pressure streamwise distribution for the two classes are reported in figure 4. The streamwise conditional pressure profiles and the difference between the both are plotted respectively in figure 4(a) and 4(b). The dimensionless longitudinal coordinate is defined by $X_{cond}^* = (x - X_{0,cond})/L$, where $X_{0,cond}$ is the mean position of the head-shock foot related to the classes. The main values $P_C^* = (P_C - P_0)/P_0$, where P_C is the average values of the conditional pressures, is shown in figure 4(a) by the dashed line for the shallowest mean interaction, and full line for the other case. In the head-shock frame, the intermittent pressure fluctuations are no longer seen and the remaining low frequency fluctuations should be associated

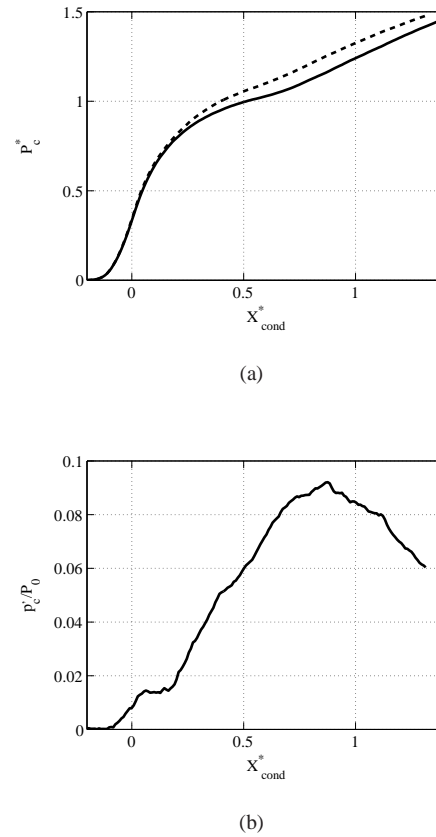


Fig. 4. Conditional mean pressure; (a) streamwise distributions, Solid line: large bubbles; dashed line: shallow bubbles; (b) difference between the profiles.

with the low frequency breathing of the separated region. These coherent fluctuations, denoted p'_C are defined as the difference between the two conditional mean pressures.

In the beginning of the interaction, the streamwise mean profiles are superimposed with each others, see figure 4(a), and the coherent fluctuations are very weak. Therefore the the shock intensity remains constant whatever the interaction length. From $X_{cond}^* = 0.2$ to 0.6 (zone B) the difference between the mean pressure profiles increase monotonically: the pressure values are higher in shallow-bubble case. In the region C, i.e X_{cond}^* between 0.6 and 1.2 , the maximum coherent-fluctuation value is reached, such as $p'_C/P_0 \approx 0.09$. Note that this value is approximately 4 times larger than the one obtained in the low-pass-filtered pressure fluctuation plotted in figure 1 (about 25×10^{-3}): this compares well with the maximal amplitudes defined as $\pm 3 \times p'_{LF}$ in the case of a Gaussian variable. Further downstream, the coherent-fluctuation values decrease.

From these conditional analysis of the wall pressure, some typical properties of the low frequency pressure fluctuations can be derived. As the head-shock intensity remains nearly constant during its displacement, the initial part of the interaction can be approximated as a simple translation of the separation point with a nearly constant flow deviation, the shock following this displacement. The pressure gradient in this region remains low, despite the fact that no clear isobaric region (or pressure plateau) can be observed for the present conditions.

On the opposite, the second part of the interaction

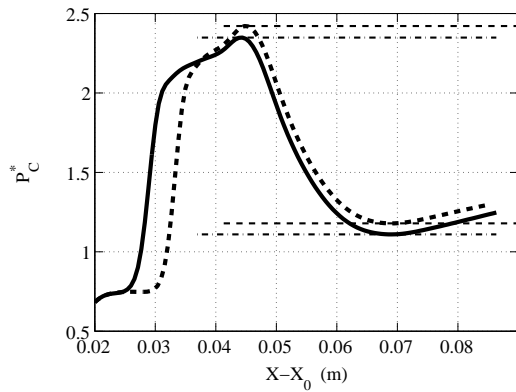


Fig. 5. Conditional mean pressure. Solid line: large bubbles; dashed line: shallow bubbles obtained at $y/H_I = 1.3$.

(region C) can be associated with larger pressure gradient and turbulent pressure fluctuations. These fluctuations can therefore influence significantly the downstream conditions of the separation shock. Nevertheless, the supersonic part of the interaction defines the regions of the shock which can be influenced due to the direction of propagation of the pressure fluctuations along the characteristics (see Agostini *et al.*, 2012).

In order to extend these results to the whole field, the same conditional analyse was carried out at the altitude $y/H_I = 1.3$, in the supersonic-flow part of the interaction. The mean pressure profiles are plotted in figure 5. It was shown that in the second part of the bubble, the level pressure is increasing when the detachment region is reducing. This increase of the pressure at the wall is also observed in the supersonic region of the interaction, see figure 5. This is due to the formation of low frequency unsteady compression waves just upstream the expansion fan, as it can be seen in the figure 3(a). From figure 5, it is clear that the expansion wave, downstream of the compression waves, does not compensate for the associated pressure fluctuations. Therefore, pressure variations similar to the pressure fluctuations produced by the variations of the compression waves intensity are observed in the downstream part of the interaction, as shown in figure 3(a).

In figure 6, a conceptual model of the streamwise wall-pressure distribution derived from the previous observations is proposed. The two classes of interaction size are respectively shown as dashed line for the shallowest interaction and as full line for the largest one. This model defines specific pressure evolutions for the three zones A, B and C:

- in the first part of the interaction, region A, the pressure-gradient magnitude associated to the head-shock remains the same whatever the interaction size, the pressure variations generated within this zone are produced only by the shock displacements (intermittent fluctuations)
- the middle interaction part, zone B, is a “buffer region” between zones A and C. In this region a “plateau” evolution with a constant pressure value P_1^S is reported for the shallowest interaction. As mentioned before, in the present case the interaction is not strong enough to observe it clearly. In this buffer region, the “intermittent” and “coherent” pressure occur. As both their natures

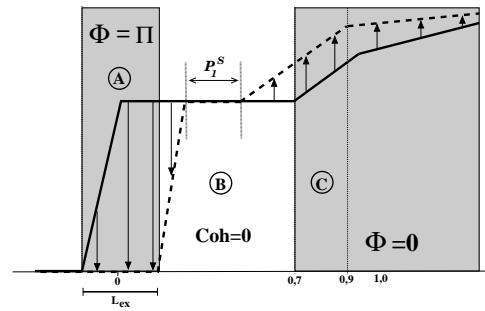


Fig. 6. Conceptual model of the streamwise wall-pressure distribution the interaction extent, in the wind-tunnel coordinate system versus; (dashed line) shallowest interaction, and (full line) the largest interaction.

and sign evolutions are different, the coherent coefficient is null.

- in the downstream part, region C, the pressure level is higher when the length of interaction is smaller. It implies that the out-of-phase relationship observed previously between regions A and C is reproduced by this scheme.

This conceptual model enables to link the low frequency streamwise pressure evolution to the interaction length fluctuations. In Piponniau *et al.* (2008), the low frequency unsteadiness breathing of the separation bubble where related to the dynamics of the convective structures produced by the shear layer induced by the decelerated region. These organized convective structures are associated with Strouhal numbers ranging from 0.5 to 1.0, typically one order of magnitude higher than the low frequency shock motion. These structures convect with a supersonic velocity relative to the supersonic side of the interaction. Therefore, the pressure disturbances generated by the convective structures follow particular paths, as shown in Agostini *et al.* (2011, 2012) and can only influence specific regions of the head-shock. This is illustrated in figure 7 where the medium frequency ($S_L = 0.5$) coherency between the head-shock displacements and wall-pressure fluctuations is presented, in the same manner as in figure 2. The following results can be observed:

- in the first part of the interaction (region B), the structures produced by the shear layer are convected and the pressure disturbances affects the head-shock dynamics. Throughout their displacements in the region $X^* < 0.5$, the pressure fluctuations produced by the convective structures influence the region below the crossing point between the head shock and the expansion wave.
- in the second part of the interaction, region C, the wall-pressure variations and the head-shock dynamics have the strongest coherence level at high altitude.

The convective structures develops along the isobaric region B and then cross the adverse pressure gradient of the region C. The initial part of this region is located at the reflection of the incident shock upon the shear layer. As detailed in Agostini *et al.* (2012), any modulation of the upstream conditions in this region will affect the reflection of the shock in compression waves in order to balance the pressure fields imposed by the subsonic region. Therefore medium frequencies fluctuations due to the convective structure should generate unsteadiness of the compression waves at the same frequencies. This is illustrated in fig-

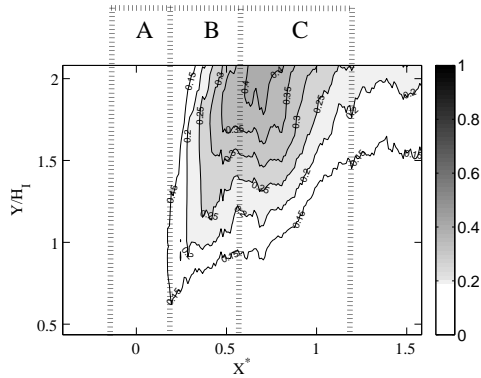


Fig. 7. Coherence-coefficient map between wall pressure fluctuations and shock position in several altitudes; at $S_L \approx 0.5$.

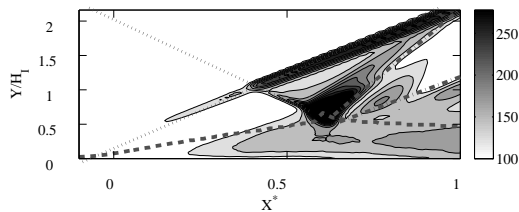


Fig. 8. standard deviation of pressure fluctuation occurring at medium frequencies $0.1 < S_L < 1$

ure 8 where rms pressure values for medium frequencies ($0.1 < S_L < 1$) are reported: it is clear that the region of compression waves emanating from the incident shock reflection present large value of pressure fluctuations in this range of frequency.

Conceptual model of equivalent inviscid interaction.

An equivalent inviscid scheme has been derived to describe these results. It is sketched in figure 9. The motion of the upstream part of the separated region is described as a simple corner translation, hence the shock induced by this flow deviation moves with an almost constant intensity. The second part of the separated zone is the source of pressure fluctuations at low frequency which influence the supersonic region. This second part is described as a second unsteady flow deviation, depending on the bubble size. This inviscid equivalent model can be extended by taking into account the medium-frequency unsteadiness. This can be achieved by associating the medium frequency unsteadiness of the second ramp with the pressure variations due to the interaction between the convective structures and the adverse pressure gradient of region C.

Therefore the second ramp, associated with the region C in the scheme sketched in figure 9, oscillates with two characteristic frequencies:

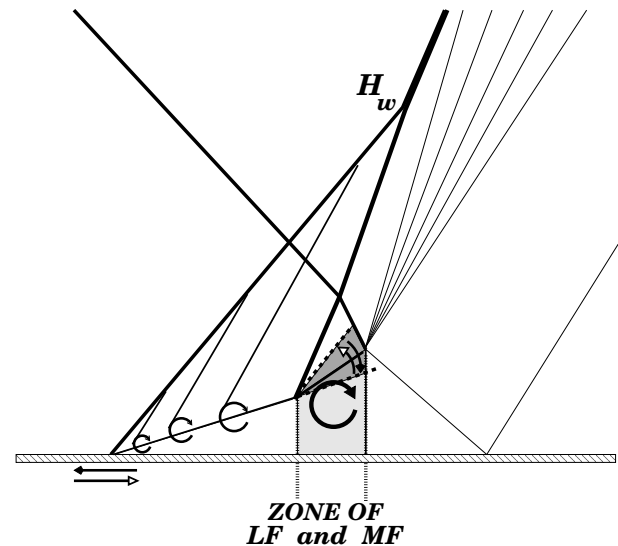


Fig. 9. Inviscid equivalent scheme for the low and medium frequency unsteadiness in the interaction.

- a low one ($S_L \approx 0.03$), associated with the bubble breathing,
- a medium one ($S_L \approx 0.5$), associated with the interaction between the convective structures and the adverse pressure gradient of the region C, near the reflection of the incident shock.

This simple scheme suggests that it is possible to relate the medium-frequency unsteadiness of the separation region to the dynamics of the convective coherent structures developing inside the mixing layer by taking into account a specific behaviour in the vicinity of the reflection of the incident shock upon the shear layer. These structures emanate from the separation point whose location follows the low frequency breathing of the separation region: the pressure gradient in the second part of the interaction increases when the bubble is contracting and vice versa. The resulting unsteady pressure field at low and medium frequency compare well with pressure fields obtained from LES In particular, the phase relationships, the coherence maps and the pressure standard deviation are accurately derived.

No direct link between the low frequency unsteadiness of the interaction and the medium frequency convective structures of the mixing layer have been established until now. Nevertheless, several authors, including, for compressible separations, Piponniau *et al.* (2009); Priebe & Martin (2012) and, for subsonic flows, Cherry *et al.* (1984); Kiya & Sasaki (1985); Ehrenstein & Gallaire (2008), have already suggested that the two phenomena have to be related. Whatever the precise mechanism, the simple inviscid scheme that is proposed here will describe accurately the whole field of unsteady pressure in the interaction.

Conclusion

Large Eddy Simulations of a Mach 2.3 shock reflection on a turbulent boundary layer have been achieved for flow deviations leading to separated interactions. The numerical results have been shown to describe accurately the low and medium frequency unsteadiness of the flow in respect with experimental data obtained in the same aerodynamic conditions.

Spectral and conditional analyses of the pressure fields

August 28 - 30, 2013 Poitiers, France

have given a global overview of the space-time organisation of the flow, and enable the derivation of an equivalent inviscid scheme. The overall of the pressure-variation properties is reproduced. This conceptual model sketches the origins of the shock system unsteadiness at low frequencies ($S_L = 0.03$) as well as medium frequencies ($S_L = 0.5$).

The motion of the upstream part of the separated region is described as a simple corner translation, hence the shock induced by this flow deviation moves with an almost constant intensity. The second part of the separated zone is the source of pressure fluctuations which influence the supersonic part of the interaction. This second part is described as a second unsteady flow deviation, sketched in the inviscid model by a ramp which imposed a flow deviation at low frequency as well as at medium frequency. The flow deviation depends on the bubble size and on the interaction between the coherent convective structures and the pressure gradient near the reflection of the incident shock wave.

This scheme explains the different regions identified from the rms pressure fields and coherence with the shock motions. Moreover, it suggests that the separation shock experiments only translational motions, with negligible intensity variations. Nevertheless, in a region located above the intersection with the incident shock, the intensity of the head-shock is increased due to the merging of unsteady pressure waves emanating from the shedding region for both low and medium frequencies. These waves generate unsteady pressure fluctuations downstream the expansion wave in phase with the head-shock displacements.

A coupling between the long-term variation of the pressure gradient associate to the low frequency modulations of the second ramp with the short-term variation of convective structure can be expected. It seems therefore that a detailed space-time description of these convective structures could be a key point for understanding the low-frequency unsteadiness in separated flows, in compressible as well as incompressible cases. Indeed, the shock-system unsteadiness has been revealed as a simple mirror of separated-zone dynamics.

Acknowledgment

Computing resources for the LES computation were provided by GENCI-IDRIS under the allocation 2009-021877

REFERENCES

- Agostini, L., Dupont, P., Larcheveque, L. & Dussauge, J.P. 2011 *International Journal of Engineering Systems Modelling and Simulation* **3** (1), 46–52.
- Agostini, Lionel, Larchevèque, Lionel, Dupont, Pierre, Debiève, Jean-François & Dussauge, Jean-Paul 2012 *AIAA Journal* **50**, 1377–1387.
- Cherry, N. J., Hillier, R. & Latour, M. E. M. P. 1984 *Journal of Fluid Mechanics* **144**, 13–46.
- Dupont, P., Haddad, C. & Debiève, J. F. 2006 *Journal of Fluid Mechanics* **559**, 255–277.
- Dupont, P., Piponniau, S., Sidorenko, A. & Debiève, J. F. 2008 *AIAA Journal* **46** (6), 1365–1370.
- Ehrenstein, U. & Gallaire, F. 2008 *Journal of Fluid Mechanics* **614**, 315–327.
- Ganapathisubramani, B., Clemens, N. T. & Dolling, D. S. 2006 *Journal of Fluid Mechanics* **556**, 271–282.
- Ganapathisubramani, B., Clemens, N. T. & Dolling, D. S. 2007 *Journal of Fluid Mechanics* **585**, 369–394.
- Kiya, M. & Sasaki, K. 1985 *Journal of Fluid Mechanics* **154** (-1), 463–491.
- Piponniau, S., Dussauge, J. P., Debiève, J. F. & Dupont, P. 2008 In *Ictam 2008*.
- Piponniau, S., Dussauge, J. P., Debiève, J. F. & Dupont, P. 2009 *Journal of Fluid Mechanics* **629**, 87–108.
- Plotkin, K.J. 1975 *AIAA Journal* **13** (8), 1036–1040.
- Priebe, S. & Martin, M. P. 2012 *Journal of Fluid Mechanics* **FirstView** (1-49).
- Robinet, J.C. 2007 *Journal of Fluid Mechanics* **579** (1), 85–112.
- Touber, E. & Sandham, N.D. 2011 *Journal of Fluid Mechanics* **671** (3), 417–465.
- Wu, M. & Martin, M. P. 2008 *Journal of Fluid Mechanics* **594**, 71–83.